Journal of Materials Science & Nanotechnology
Volume 10 | Issue 1
ISSN: 2348-9812

Research Article
Open Access

# 2D Analysis of Piezoelectric Layer Over a Rotating Micro-elongated Thermoelastic Medium with DPL Model

**Othman MIA*[1], Atwa SY[2], Eraki EEM[1], Ismail MF[2]**

[1]Department of Mathematics, Faculty of Science, Zagazig University, P.O. Box 44519, Zagazig, Egypt.
[2]Department of Engineering Mathematics and Physics, Higher Institute of Engineering, Shorouk Academy, Egypt

*Corresponding Author: Othman MIA, Department of Mathematics, Faculty of Science, Zagazig University, P.O. Box 44519, Zagazig, Egypt. Tel: 1112320891, Email: m_i_a_othman@yahoo.com

**Citation:** Othman MIA, Atwa SY, Eraki EEM, Ismail MF (2022) 2D Analysis of Piezoelectric Layer Over a Rotating Micro-elongated Thermoelastic Medium with DPL Model. J Mater Sci Nanotechnol 10(1): 102

## Abstract

The Lord-Shulman theory with one relaxation time and the dual-phase-lag model with two relaxation times of thermo-elasticity are used in this article to study the influence rotation micro-elongated thermoelastic layer, when a piezo electric layer is above it. To convert a partial differential equation to an ordinary differential equation, the normal mode method is utilized. Numerical computations are implemented for aluminum epoxy, and the results are charted. A comparison is made among the two theories in the complete absence and the presence of a rotation. The presence of a rotation has a major effect on all physical quantities.

**Keywords:** Piezoelectric, Normal Mode Analysis, Rotation, Dual-Phase-Lag Model, Micro-Elongated Thermo elasticity

**Nomenclature**

| | |
|---|---|
| $T$ | Absolute temperature |
| $\boldsymbol{\Omega}$ | Angular velocity |
| $\alpha_{t_1}$ , $\alpha_{t_2}$ | Coefficient of linear thermal expansion where $\beta_0 = (3\lambda + 2\mu)\alpha_{t_1}$, $\beta_1 = (3\lambda + 2\mu)\alpha_{t_2}$ |
| $\sigma_{ij}$ | Component of stress tensor for micro-elongated medium |
| $\rho$ | Density in micro-elongated medium |
| $\rho^P$ | Density in piezoelectric layer |
| $\boldsymbol{u}$ | Displacement vector in micro-elongated medium |
| $\boldsymbol{u}^p$ | Displacement vector in piezoelectric layer |
| $E_i$ | Electric field in piezoelectric layer |
| $\tau_q$ | Heat flux parameter |
| $\lambda, \mu$ | Lame's constants in micro-elongated medium |
| $a_0, \lambda_0, \lambda_1$ | Micro-elongational constants |

| | |
|---|---|
| $\varphi$ | Micro-elongational scalar |
| $j_0$ | Microinertia |
| $T_0$ | Reference temperature |
| $c_e$ | Specific heat at constant strain in micro-elongated medium |
| $c_e^P$ | Specific heat at constant strain in piezoelectric layer |
| $\tau_\theta$ | Temperature gradient parameter |
| $\in_{ij}$ | The dielectric moduli in piezoelectric layer |
| $C_{ijkl}$ | The elastic parameters tensor in piezoelectric |
| $D_i$ | The electric displacement in piezoelectric layer |
| $\varphi^p$ | The electric potential in piezoelectric layer |
| $e_{kij}$ | The piezo electric moduli in piezoelectric layer |
| $k$ | Thermal conductivity in micro-elongated medium |
| $k^p$ | Thermal conductivity in piezoelectric layer |

## Introduction

Piezoelectric is the conversion of mechanical stress to electrical charge, and vice versa. Piezoelectric substances are produced industrially in single-crystal and ceramic shapes, and they are the second most common application of dielectric materials, after semiconductor materials (Othman et al. [1]). Based on observation distribution generated electric potential difference throughout the disk thickness, Ashida and Tauchert [2] proposed a finite-difference composition for assessing the time-varying, axisymmetric ambient temperature on the face of a piezoelectric circular disk. In the 2006 Haussuhl et al. [3] proposed Bismuth triborate (BiB3O6) is a nonlinear optical material with piezo-electric and elastic properties. Li and He [4] recently introduced the study of a general linear piezoelectric-thermoelastic problem with a nonlocal influence and temperature-dependent characteristics.

A micro-elongated elastic solid has four degrees of freedom, three of which are for translation and one for micro-elongation. According to micro-elongation theory, material particles can really only carry out volumetric micro elongation in addition to classical medium deformation. Such medium's material points can lengthen and contract independently of their translations. And also, micro-elongated media include solid liquid crystals, composite materials reinforced with chopped elastic fibers, and porous media with pores filled with non-viscous fluid or gas. In the context of generalized thermo-elastic theory, Shaw and Mukhopadhyay [5] examined the response due to periodically differing heat sources in vicinity of the origin of a functionally graded isotropic boundless micro-elongated medium in 2012. One year later, Shaw and Mukhopadhyay [6] again presented another study to investigate the implications of a moving heat source in an infinitely long micro-elongated, isotropic, homogeneous, thermoelastic medium. In 2015, Sachdeva and Ailawalia [7] presented research on two-dimensional deformation in a thermoelastic micro-elongated solid, when mechanical force applied along the user interface of fluid half-space and thermoelastic micro-elongated half-space. Also, in the same year, Ailawalia et al. [8] focused on to study the deformation caused by an internal heat source in a thermoelastic micro-elongated solid with an h-thick elastic layer on top. later, Ailawalia et al. [9] reintroduced the previous study in a different way, where he changes the elastic layer from a bounded layer to an unbounded layer. Utilizing the normal mode analysis technique, Ailawalia et al. [10] developed a model for a thermoelastic micro elongated solid keep in mind the micro elongation effect and laser pulse heating. The eigenvalue approach was used to solve an axisymmetric problem of a micro-elongated thermoelastic medium with an infinite circular plate under the effect of thermo-mechanical sources has been discussed by Kumar et al. [11]. Ailawalia and Singla [12] studied two-dimensional deformation caused by laser pulse heating in a thermoelastic micro elongated layer with a thickness of 2d that is engrossed an infinite inviscid liquid.

Ozisik and Tzou [13] and Tzou [14, 15] developed a new model for the heat transport mechanism named the dual-phase-lag model, in which Fourier's law is replaced by an approximation to the modification of Fourier's law with two different time translations for the heat flux and the temperature gradient. In the dual-phase-lag model, Othman and Abd-Elaziz [16] focused on investigation the influence of thermal loading caused by laser pulses on thermoelastic medium with voids. Abbas [17] published a research paper to examine the influence of dual-phase-lag on thermoelastic interplay in an infinite fiber-reinforced anisotropic medium with a circular hole. Reflection of plane waves from electro-magneto-thermoelastic half-space using a dual-phase-lag model has been discussed by Abd-Alla et al. [18]. Othman and Abd-Elaziz [19] utilized a dual-phase-lag model to investigate the effect of gravitational and rotation fields on the plane waves of a linearly magneto-micropolar thermoplastic isotropic medium. Based on the dual-phase-lag modification of Fourier's law, Othman and Eraki [20] studied the induced thermo-elastic diffusion waves in a homogeneous isotropic medium due to an ultra-short-pulsed laser heating that decomposed significantly. Abdou et al. [21] explained the effect of rotation and gravity on generalized thermoelastic medium with double porosity under L-S theory.

In the background of Green and Lindsay's linearized theory, Othman [22] provided the normal mode analysis to two-dimensional problems of general linear thermoelasticity with two relaxation times under the influence of rotation. Othman [23] proposed a generalized thermo-viscoelastic plane wave model for a half-space whose surface is subjected to a thermal shock under the influence of rotation with one relaxation time. Othman and Singh [24] discussed the influence of rotation on general linear micropolar thermoelasticity in a half-space according to five theories. Othman and song [25] studied the rotational effects on general linear electro-magneto-thermo-viscoelasticity plane waves with two relaxation times. Later, Li et al. [26] proposed to investigate the rotational influences on plane waves of general linear electro-magneto-thermoelastic with diffusion in a half-space. Othman and Abbas [27] provided the multi-phase-lag theory in order to investigate the rotating on a 2-D analysis of the micropolar thermoelastic isotropic medium.

The main objective of this paper is to examine the influence rotation micro-elongated thermoelastic layer under dual-phase-lag model, when piezo electric layer is above it. The precise expression of the variables examined for the dual-phase-lag model of thermo-elasticity and the variation of the variables examined are depicted graphically using normal mode analysis.

## Formulation of the Problem

The system of governing equations of a micro-elongated thermoelasticity with rotation, in a dual-phase-lag model (Fig. 1) can be written as [8, 12]

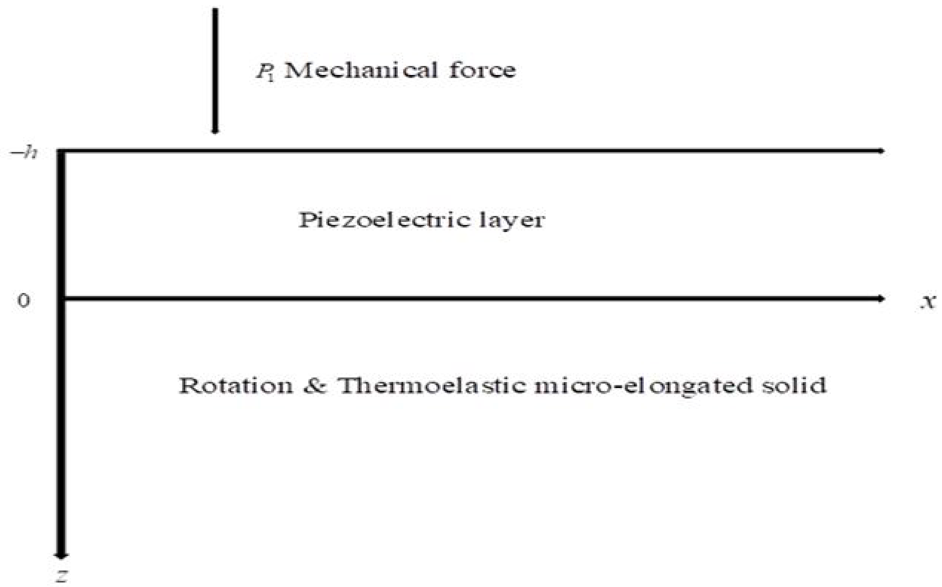


**Figure 1:** Geometry of the problem

$$\sigma_{ij,j} = \rho[u_{i,tt} + \{\boldsymbol{\Omega}\times(\boldsymbol{\Omega}\times\boldsymbol{u})\}_i + (2\boldsymbol{\Omega}\times\boldsymbol{u}_{,t})_i], \tag{1}$$

$$a_0\varphi_{,ii} + \beta_1 T - \lambda_1\varphi - \lambda_0 u_{j,j} = \frac{1}{2}\rho j_0 \varphi_{,tt}, \tag{2}$$

$$k\,(1+\tau_\theta\frac{\partial}{\partial t})T_{,ii} = (1+\tau_q\frac{\partial}{\partial t})(\rho c_e\frac{\partial T}{\partial t} + \beta_0 T\, u_{k,kt}) + \beta_1 T_0\varphi_{,t}, \tag{3}$$

$$\sigma_{ij} = 2\mu\varepsilon_{ij} + (\lambda e - \beta_0 T + \lambda_0\varphi)\delta_{ij}. \tag{4}$$

From equation (1) and equation (4) for displacement vector $\boldsymbol{u}(x,z,t) = u(u_1,0,u_3)$, and the rotation $\boldsymbol{\Omega}=(0,\Omega,0)$ the equations of motion are given by.

$$\mu\nabla^2 u_1 + (\lambda+\mu)e_{,x} - \beta_0 T_{,x} + \lambda_0\varphi_{,x} = \rho(u_{1,tt} - \Omega^2 u_1 + 2\Omega u_{3,t}), \tag{5}$$

$$\mu\nabla^2 u_3 + (\lambda+\mu)e_{,z} - \beta_0 T_{,z} + \lambda_0\varphi_{,z} = \rho(u_{3,tt} - \Omega^2 u_3 + 2\Omega u_{1,t}). \tag{6}$$

For simplification we shall use the following non-dimensional variables

$$x_i' = \frac{\omega^*}{c_1}x_i,\ \ z' = \frac{\omega^*}{c_1}z,\ \ u_i' = \frac{\omega^*\rho c_1}{\beta_0 T_0}u_i,\ \ u_i^{e'} = \frac{\omega^*\rho c_1}{\beta_0 T_0}u_i^e,\ \ t' = \omega^* t,\ \ \tau_\theta' = \omega^*\tau_\theta,\ \ \tau_q' = \omega^*\tau_q,\ \ \sigma_{ij}' = \frac{\sigma_{ij}}{\beta_0 T_0},$$

$$\sigma_{ij}^{e'} = \frac{\sigma_{ij}^e}{\beta_0 T_0},\ \ \varphi' = \frac{\lambda_0}{\beta_0 T_0}\varphi,\ \ T' = \frac{T}{T_0},\ \ \Omega' = \frac{\Omega}{\omega^*},\ \ P_1' = \frac{P_1}{\beta_0 T_0},\ \ \omega^* = \frac{\rho c_1^2 c_e}{k},\ \ c_1^2 = \frac{\lambda+2\mu}{\rho}. \tag{7}$$

The displacement potentials $\Phi(x,z,t)$ and $\psi(x,z,t)$ which relate to displacement components has been introduced, we obtain

$$u_1 = \Phi_{,x} + \psi_{,z},\qquad u_3 = \Phi_{,z} - \psi_{,x}. \tag{8}$$

Substituting from Eqs. (7) and (8) into Eqs. (2), (3), (5) and (6), we obtain

$$[(a_1+a_2)\nabla^2 + \Omega^2 - \frac{\partial^2}{\partial t^2}]\Phi + 2\Omega\psi_{,t} - T + \varphi = 0, \tag{9}$$

$$-2\Omega\Phi_{,t} + (a_1\nabla^2 + \Omega^2 - \frac{\partial^2}{\partial t^2})\psi = 0, \tag{10}$$

$$-a_5\nabla^2\Phi + a_3 T + (\nabla^2 - a_4 - a_6\frac{\partial^2}{\partial t^2})\varphi = 0, \tag{11}$$

$$-a_8(1+\tau_q\frac{\partial}{\partial t})\nabla^2\Phi_{,t} + (1+\tau_\theta\frac{\partial}{\partial t})\nabla^2 T - a_7(1+\tau_q\frac{\partial}{\partial t})T_{,t} - a_9\varphi = 0. \tag{12}$$

## The Normal Mode Analysis

The solution of the considered physical variable can be decomposed in terms of normal modes as the following form:

$$[u_i,\varphi,T,\psi,\Phi,\sigma_{ij},u_i^p,\sigma_{ij}^p,D_i](x,z,t) = [u_i^*,\varphi^*,T^*,\psi^*,\Phi^*,\sigma_{ij}^*,u_i^{p*},\sigma_{ij}^{p*},D_i^*](z)e^{(\omega t+ibx)}, \tag{13}$$

where, $\omega$ is a complex constant, $i=\sqrt{-1}$, $b$ is wave number in the $x$ direction.

Using Eq. (13) into Eqs. (9)-(12), then we have

$$(a_{10} D^2 + a_{11}) \Phi^* + 2\Omega\omega\psi^* - T^* + \varphi^* = 0, \tag{14}$$

$$-2\Omega\omega \Phi^* + (a_1 D^2 + a_{12})\psi^* = 0, \tag{15}$$

$$(-a_5 D^2 + a_{13}) \Phi^* + a_3 T^* + (D^2 - a_{14})\varphi^* = 0, \tag{16}$$

$$(-a_{17} D^2 + a_{18}) \Phi^* + (a_{16} D^2 - a_{19}) T^* - a_9 \omega\varphi^* = 0. \tag{17}$$

Eqs. (14-17) have a non-trivial solution if the determinant coefficients of the physical quantities equal to zero, then we get.

$$(D^8 - A D^6 + B D^4 - C D^2 + E)\{\Phi^*(z), \psi^*(z), T^*(z), \varphi^*(z)\} = 0. \tag{18}$$

Eq. (18) can be factorized as:

$$(D^2 - k_1^2)(D^2 - k_2^2)(D^2 - k_3^2)(D^2 - k_4^2)\{\Phi^*(z), \psi^*(z), T^*(z), \varphi^*(z)\} = 0. \tag{19}$$

Where, $k_n^2, (n = 1,2,3,4)$ are roots of the characteristic equation of Eq. (19)

The general solutions of Eq. (19) bound as $(z \to \infty)$ is given by.

$$(\Phi^*, \psi^*, T^*, \varphi^*)(z) = \sum_{n=1}^{4} (1, H_{1n}, H_{2n}, H_{3n}) M_n e^{-k_n z}. \tag{20}$$

Substituting from Eq. (20) into Eq. (8) we obtain the components of displacements.

$$u_1^*(z) = \sum_{n=1}^{4} (ib - k_n H_{1n}) M_n e^{-k_n z}, \tag{21}$$

$$u_3^*(z) = \sum_{n=1}^{4} -(k_n + ibH_{1n}) M_n e^{-k_n z}. \tag{22}$$

Substituting from Eqs. (7) and (13) into (4) and with the help of Eqs. (20-22) we obtain the components of stresses.

$$(\sigma_{xx}^*, \sigma_{zz}^*, \sigma_{xz}^*)(z) = \sum_{n=1}^{4} (H_{4n}, H_{5n}, H_{6n}) M_n e^{-k_n z}, \tag{23}$$

where, the coefficient $a_i$, $A, B, C, E$ and $H_{in}$ are given in Appendix 1.

The system of governing equations of general piezoelectric are given by [28-30]

$$\sigma_{ij,j}^p = \rho^p u_{i,tt}^p, \tag{24}$$

$$D_{i,i} = 0, \tag{25}$$

$$\sigma_{ij}^p = \frac{1}{2} C_{ijkl} (u_{k,l}^p + u_{l,k}^p) - e_{kij} E_k, \tag{26}$$

$$D_i = \frac{1}{2} e_{ijk} (u_{j,k}^p + u_{k,j}^p) + \in_{ij} E_j, \tag{27}$$

where, $E_i = -\varphi_{,i}^p$.

For simplification, we shall use the following non-dimensional variables [4]

$$x^{p'}=c_0\eta_0 x^p,\quad z^{p'}=c_0\eta_0 z^p,\quad u_i^{p'}=c_0\eta_0 u_i^p,$$

$$t^{p'}=c_0^2\eta_0 t^p,\quad \sigma_{ij}^{p'}=\frac{\sigma_{ij}^p}{C_{11}},\quad D_i'=\frac{D_i}{e_{33}},\quad \varphi^{p'}=\frac{\in_{11}c_0\eta_0}{e_{33}}\varphi^p,\quad c_0^2=\frac{c_{11}}{\rho^p},\quad \eta_0=\frac{\rho^p c_e^p}{k^p}. \tag{28}$$

Substituting from Eqs. (28) and (13) into Eqs. (24) and (25)

$$(l_1 \mathrm{D}^2 - A_1)u_1^{p*} + i\,b\,l_2\,\mathrm{D}u_3^{p*} + i\,b\,l_3\,\mathrm{D}\varphi^{p*}=0, \tag{29}$$

$$i\,b\,l_2\,\mathrm{D}u_1^{p*} + (l_5\mathrm{D}^2 - A_2)u_3^{p*} + (l_7\mathrm{D}^2 - b^2 l_6)\varphi^{p*}=0, \tag{30}$$

$$i\,b\,l_8\,\mathrm{D}u_1^{p*} + (\mathrm{D}^2 - b^2 l_9)u_3^{p*} + (-l_{10}\mathrm{D}^2 + b^2)\varphi^{p*}=0. \tag{31}$$

Eliminating $u_1^{p*}, u_3^{p*}, \varphi^{p*}$ between Eqs. (29), (30) and (31), we obtain

$$(\mathrm{D}^6 - G\,\mathrm{D}^4 + N\,\mathrm{D}^2 - F)\{u_1^{p*}(z), u_1^{p*}(z), \varphi^{p*}(z)\}=0. \tag{32}$$

Eq. (32) can be factorized as:

$$(\mathrm{D}^2 - r_1^2)(\mathrm{D}^2 - r_3^2)(\mathrm{D}^2 - r_3^2)\{u_1^{p*}(z), u_1^{p*}(z), \varphi^{p*}(z)\}=0. \tag{33}$$

Where, $r_m^2, (m=1,2,3)$ are roots of the characteristic equation of Eq. (33) the solutions of Eq. (33) are of the form:

$$(u_1^{p*}, u_3^{p*}, \varphi^{p*})(z)=\sum_{m=1}^{3}(1, L_{1m}, L_{2m})R_m e^{-r_m z} + \sum_{m=1}^{3}(1, L_{1(m+3)}, L_{2(m+3)})R_{m+3} e^{r_m z}. \tag{34}$$

Substituting from Eqs. (28) and (13) into Eqs. (26) and (27) and with the help of Eq. (34),

we obtain the components of stresses and the electric displacement in a piezoelectric layer

$$(\sigma_{xx}^{p*}, \sigma_{zz}^{p*}, \sigma_{xz}^{p*})(z)=\sum_{m=1}^{3}(L_{3m}, L_{4m}, L_{5m})R_m e^{-r_m z} + \sum_{n=1}^{3}(L_{3(m+3)}, L_{4(m+3)}, L_{5(m+3)})R_{(m+1)} e^{r_n z}, \tag{35}$$

$$(D_x^*, D_z^*)(z)=\sum_{m=1}^{3}(L_{6m}, L_{7m})R_m e^{-r_m z} + \sum_{m=1}^{3}(L_{6(m+3)}, L_{7(m+3)})R_{m+3} e^{r_m z}. \tag{36}$$

The coefficient $l_{m'}$, $A_1$, $A_2$, $G, N, F, H_{n'n}$ and

$L_{m'm}$, $L_{m'(m+3)}$, where $m'=1,2,....,7$ and $n'=1,2,.....,6$ are given in Appendix 2

## The Boundary Condition

The parameters $M_n$, $(n = 1,2,3,4)$, $R_m$ and $R_{m+3}$, $(m = 1,2,3)$ have to be selected such that boundary conditions at the surface are

$$\sigma_{zz} = \sigma_{zz}^P,\ \sigma_{xz} = \sigma_{xz}^P,\ u_1 = u_1^P,\ u_3 = u_3^P,\ \varphi = 0,\ \frac{\partial T}{\partial z} = 0,\ D_x = 0,\ D_z = 0\ at\ z = 0. \tag{37}$$

$$\sigma_{zz} = \sigma_{zz}^{p} - P_1 e^{(\omega t + i b x)}, \quad \sigma_{xz} = 0, \quad \text{at} \quad z = -h. \tag{38}$$

Where, $P_1$ is the magnitude of the mechanical force.

The utilization of the expressions of the variables considered into above boundary conditions (37), (38) to obtain the equations that are satisfied by the parameters. And hence, ten equations will be obtained. If the inverse method matrix is applied on the ten equations, we get then the value constant $M_n, (n=1,2,3,4)$, $R_m$ and $R_{m+3}$, $(m=1,2,3)$.

$$\begin{bmatrix} M_1 \\ M_2 \\ M_3 \\ M_4 \\ R_1 \\ R_2 \\ R_3 \\ R_4 \\ R_5 \\ R_6 \end{bmatrix} = \begin{bmatrix} H_{51} & H_{52} & H_{53} & H_{54} & -L_{41} & -L_{42} & -L_{43} & -L_{44} & -L_{45} & -L_{46} \\ H_{61} & H_{62} & H_{63} & H_{64} & -L_{51} & -L_{52} & -L_{53} & -L_{54} & -L_{55} & -L_{56} \\ ib-k_1H_{11} & ib-k_2H_{12} & ib-k_3H_{13} & ib-k_4H_{14} & -1 & -1 & -1 & -1 & -1 & -1 \\ -k_1-ibH_{11} & -k_2-ibH_{12} & -k_3-ibH_{13} & -k_4-ibH_{14} & -L_{11} & -L_{12} & -L_{13} & -L_{14} & -L_{15} & -L_{16} \\ H_{31} & H_{32} & H_{33} & H_{34} & 0 & 0 & 0 & 0 & 0 & 0 \\ -k_1H_{21} & -k_2H_{22} & -k_3H_{23} & -k_4H_{24} & 0 & 0 & 0 & 0 & 0 & 0 \\ 0 & 0 & 0 & 0 & -L_{61} & -L_{62} & -L_{63} & -L_{64} & -L_{65} & -L_{66} \\ 0 & 0 & 0 & 0 & -L_{71} & -L_{72} & -L_{73} & -L_{74} & -L_{75} & -L_{76} \\ H_{51}e^{k_1h} & H_{52}e^{k_2h} & H_{53}e^{k_3h} & H_{54}e^{k_4h} & -L_{41}e^{r_1h} & -L_{42}e^{r_2h} & -L_{43}e^{r_3h} & -L_{44}e^{-r_1h} & -L_{45}e^{-r_2h} & -L_{46}e^{-r_3h} \\ H_{61}e^{k_1h} & H_{62}e^{k_2h} & H_{63}e^{k_3h} & H_{64}e^{k_4h} & 0 & 0 & 0 & 0 & 0 & 0 \end{bmatrix}^{-1} \begin{bmatrix} 0 \\ 0 \\ 0 \\ 0 \\ 0 \\ 0 \\ 0 \\ 0 \\ -P_1 \\ 0 \end{bmatrix} \tag{39}$$

## Numerical Results and Discussion

The analysis is conducted for aluminum epoxy-like material as [6]:

$\lambda = 7.59\times10^{10}\ \mathrm{N/m^2}$, $a_0 = 0.61\times10^{-10}\ \mathrm{N}$, $a_0 = 0.61\times10^{-10}\ \mathrm{N}$, $\rho = 2.19\times10^{3}\ \mathrm{kg/m^3}$,

$c_e = 966\ \mathrm{J/kg.k}$, $\beta_0 = \beta_1 = 0{,}05\times10^{5}\ \mathrm{N/m^2\ .k}$, $k = 252\ \mathrm{J/m.s.k}$, $j_0 = 0.196\times10^{-4}\ \mathrm{m^2}$,

$\lambda_0 = \lambda_1 = 0.37\times10^{10}\ \mathrm{N/m^2}$, $T_0 = 293\mathrm{k}$, $\tau_\theta = 0.002\ \mathrm{s}$, $0.009\mathrm{s}$, $\omega = \omega_0 + i\zeta$,

$\omega_0 = -\ 6.428\times10^{-4} S^{-1}$ $\zeta = 0.06657\ S^{-1}$, $b = 4\ \mathrm{m^{-1}}$, $h = 0.001\mathrm{m}$.

The material chosen for piezoelectric is taken as Cadmium Selenide (CdSe) having hexagonal symmetry (6 mm class) [31]

$C_{11} = 7.41\times10^{10}\ \mathrm{N.m^{-2}}$, $C_{13} = 3.93\times10^{10}\ \mathrm{N.m^{-2}}$, $C_{33} = 8.36\times10^{10}\ \mathrm{N.m^{-2}}$, $C_{44} = 1.32\times10^{10}\ \mathrm{N.m^{-2}}$, $\rho = 5504\ \mathrm{kg.m^{-3}}$, $e_{31} = -0.160\ \mathrm{C.m^{-2}}$, $e_{33} = 0.347\ \mathrm{C.m^{-2}}$, $e_{15} = -0.138\ \mathrm{C.m^{-2}}$, $c_e^{p} = 260\ \mathrm{J/kg.k}$, $\in_{11} = 8.26\times10^{-11}\ \mathrm{C^2.N^{-1}.m^{-2}}$, $\in_{33} = 9.03\times10^{-11}\ \mathrm{C^2.N^{-1}.m^{-2}}$.

The computations are implemented for the value dimensionless time $t = 0.021s$ in the range $0 \le z \le 1.4$ on the surface $x = 1.4\,\mathrm{m}$ to all physical quantities except the temperature $T$ and the micro-elongational scalar $\varphi$ is in a range $0 \le z \le 3$. The numerical technique presented here is used to distribute the horizontal displacement $u_1$, the vertical displacement $u_3$, the temperature $T$, the micro-elongational scalar $\varphi$, the stresses components $\sigma_{xx}, \sigma_{zz}$ and $\sigma_{xz}$ with distance $z$. To examine the effect of the presence and complete absence of rotation on the solution in the dual-phase-lag model and Lord-Shulman theory and the influence of the phase-lag temperature of gradient $\tau_\theta$, when the phase-lag of heat flux $\tau_q$ is constant on solution in just dual-phase-lag. This paper presents the numerical evaluation results in the form of charts. The results are depicted in Figs. 2-15 for the magnitude of mechanical force $P_1 = 10$N Figs. 2-8 exhibit the variation of the previous physical quantities with the distance $z$ in the presence and absence of rotation (i.e., $\Omega = 0.91\ S^{-1}$, $\Omega = 0$) for both the dual-phase-lag model and Lord-Shulman theory. Fig. 2 illustrates the distribution of horizontal displacement $u_1$ versus a distance $z$. It obvious that the two curves based on the dual-phase-lag model start at the same point then decreasing up to disappear at $z \geq 1.4$, moreover, there are on other two curves based on Lord-Shulman theory initiate from the same point which is different from the previous point and also decreasing up to disappear at $z \geq 1.4$. Figs. 3 and 6 clarify the values of the vertical displacement and the force stress component always initiate from positive values and decrease in the range $0 \leq z \leq 1.4$, after that go to zero in the range $z \geq 1.4$. It is also clear that the values of $u_3$ and $\sigma_{xx}$ based on the dual-phase-lag model are large compared with the values of $u_3$ and $\sigma_{xx}$ based on the Lord-Shulman theory. Figs. 4 and 5 depict the change in temperature $T$ and the micro-elongational scalar $\varphi$ with distance $z$. In the presence of rotation (i.e. $\Omega = 0.91\ S^{-1}$) the values of $T$ and $\varphi$ always start with increasing to a maximum value, then decrease and finally converge to zero. It is also seen that the values of $T$ dependent on the dual-phase-lag model are small compared with the values of $T$ dependent on the L-S theory in the case of the presence of rotation in fig. 4, while occurs the opposite in fig. 5 on the same previous case. Figs. 7 and 8 exhibit the value of the forces stresses components $\sigma_{zz}$ and $\sigma_{xz}$ always initiate from negative values and increase in the range $0 \leq z \leq 1.4$, after that go to zero in the range $z \geq 1.4$. It is evident that the values of $\sigma_{zz}$ and $z$ dependent on the dual-phase-lag model initiate from the same point which is the same point in Figs. 7 and 8. Figs. 9-15 show the variation of the previous physical quantities with the distance $z$ in the presence of rotation (i.e., $\Omega = 0.91\ S^{-1}$) for dual-phase-lag model at $\tau_q = 9 \times 10^{-5}\ S$, $\tau_\theta = 10^{-5},\ 2 \times 10^{-5},\ 3 \times 10^{-5}\ S^{-1}$. Figs. 9, 10 and 13 depict the variation of the horizontal displacement $u_1$ and the vertical displacement $u_3$ and the force stress component $\sigma_{xx}$ with distance $z$. The values of the previous physical decrease up to vanished at distance $z \geq 1.8$. It is also obvious that the influence of $T$ is an increase in Fig. 9 whereas in figs. 10 and 13 is a decrease. Fig. 11 describes the change in the temperature $T$ against distance $z$. It is clear that the values of $T$ increase when the effect of the phase-lag of temperature gradient $\tau_\theta$ increases. Fig. 12 presents the change in the micro-elongational scalar $\varphi$ with distance $z$. The three values of $\varphi$ initiate from zero then increasing to a maximum after that decrease even vanish. It is also evident that the values of $\varphi$ decrease when the influence of the phase-lag of temperature gradient $\tau_\theta$ increases. Figs. 14 and 15 exhibit the distribution of the forces stresses components $\sigma_{zz}$ and $\sigma_{xz}$ versus distance $z$. All curves begin from the negative values then increase even go to zero. In Fig. 14 the values of $\sigma_{zz}$ decrease when the phase-lag of temperature gradient $\tau_\theta$ decreasing, but in Fig. 15, the values of $\sigma_{xz}$ increase when the phase-lag of temperature gradient $\tau_\theta$ decreases. e phase-lag of heat flux $\tau_q$ is constant on solution in just dual-phase-lag. This paper presents the numerical evaluation results in the form of charts. The results are depicted in Figs. 2-15 for the magnitude of mechanical force $P_1 = 10$ N. Figs. 2-8 exhibit the variation of the previous physical quantities with the distance $z$ in the presence and absence of rotation (i.e., $\Omega = 0.91\ S^{-1}$, $\Omega = 0$) for both the dual-phase-lag model and Lord-Shulman theory. Fig. 2 illustrates the distribution of horizontal displacement $u_1$ versus a distance $z$. It obvious that the two curves based on the dual-phase-lag model start at the same point then decreasing up to disappear at $z \geq 1.4$, moreover, there are on other two curves based on Lord-Shulman theory initiate from the same point which is different from the previous point and also decreasing up to disappear at $z \geq 1.4$. Figs. 3 and 6 clarify the values of the vertical displacement and the force stress component always initiate from positive values and decrease in the range $0 \leq z \leq 1.4$, after that go to zero in the range $z \geq 1.4$. It is also clear that the values of $u_3$ and $\sigma_{xx}$ based on the dual-phase-lag model are large compared with the values of $u_3$ and $\sigma_{xx}$ based on the Lord-Shulman theory. Figs. 4 and 5 depict the change in temperature $T$ and the micro-elongational scalar $\varphi$ with distance In the presence of rotation (i.e. $\Omega = 0.91\ S^{-1}$) the values of $T$ and $\varphi$ always start with increasing to a maximum value, then decrease and finally converge to zero. It is also seen that the values of $T$ dependent on the dual-phase-lag model are small compared with the values of $T$ dependent on the L-S theory in the case of the presence of rotation in fig. 4, while occurs the opposite in fig. 5 on the same previous case. Figs. 7 and 8 exhibit the value of the forces stresses components $\sigma_{zz}$ and $\sigma_{xz}$ always initiate from negative values and increase in the range $0 \leq z \leq 1.4$, after that go to zero in the range $z \geq 1.4$. It is evident that the values of $\sigma_{zz}$ and $\sigma_{xz}$ dependent on the dual-phase-lag model initiate from the same point which is the same point in Figs. 7 and 8. Figs. 9-15 show the variation of the previous physical quantities with the distance $z$ in the presence of rotation (i.e., $\Omega = 0.91\ S^{-1}$) for dual-phase-lag model at $\tau_q = 9 \times 10^{-5}\ S$, $\tau_\theta = 10^{-5},\ 2 \times 10^{-5},\ \times 10^{-}$ Figs. 9, 10 and 13 depict the variation of the horizontal displacement $u_1$ and the vertical displacement $u_3$ and the force stress component $\sigma_{xx}$ with distance $z$. The values of the previous physical decrease up to vanished at distance $z \geq 1.8$. It is also obvious that the influence of $\tau_\theta$ is an increase in Fig. 9 whereas in figs. 10 and 13 is a decrease. Fig. 11 describes the change in the temperature $T$ against distance $z$. It is clear that the values of $T$ increase when the effect of the phase-lag of temperature gradient $\tau_\theta$ increases. Fig. 12 presents the change in the micro-elongational scalar $\varphi$ with distance $z$. The three values of $\varphi$ initiate from zero then increasing to a maximum after that decrease even vanish. It is also evident that the values of $\varphi$ decrease when the influence of the phase-lag of temperature gradient $\tau_\theta$ increases. Figs. 14 and 15 exhibit the distribution of the forces stresses components $\sigma_{zz}$ and $\sigma_{xz}$ versus distance $z$. All curves begin from the negative values then increase even go to zero. In Fig. 14 the values of $\sigma_{zz}$ decrease when the phase-lag of temperature gradient $\tau_\theta$ decreasing, but in Fig. 15, the values of $\sigma_{xz}$ increase when the phase-lag of temperature gradient $\tau_\theta$ decreases.

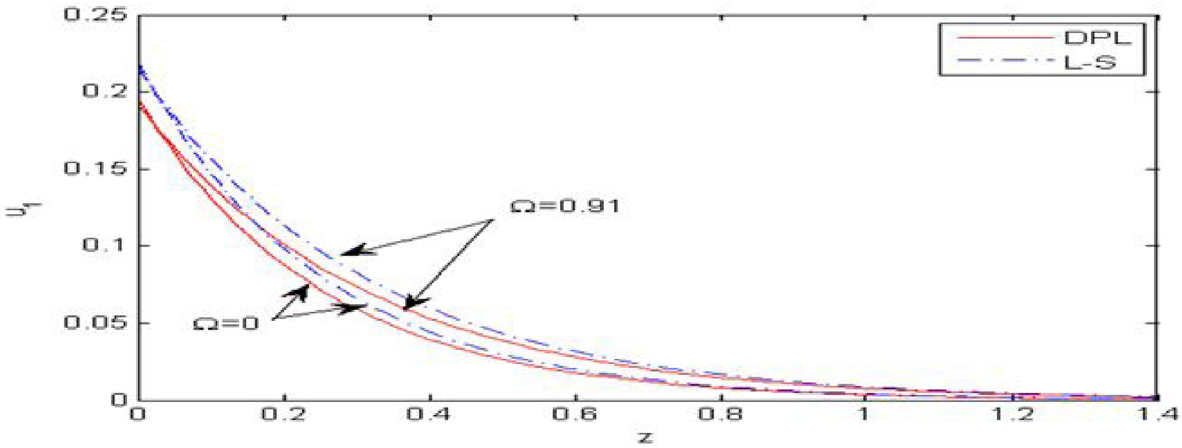


**Figure 2:** Variation of the horizontal displacement $u_1$ in the absence and presence of rotatio

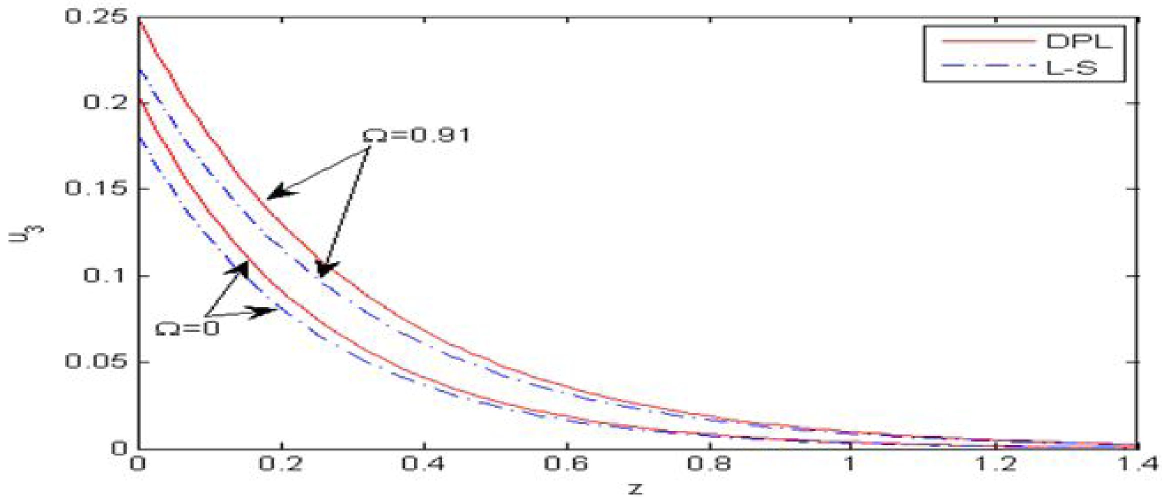


**Figure 3:** Variation of the vertical displacement $u_3$ in the absence and presence of rotation

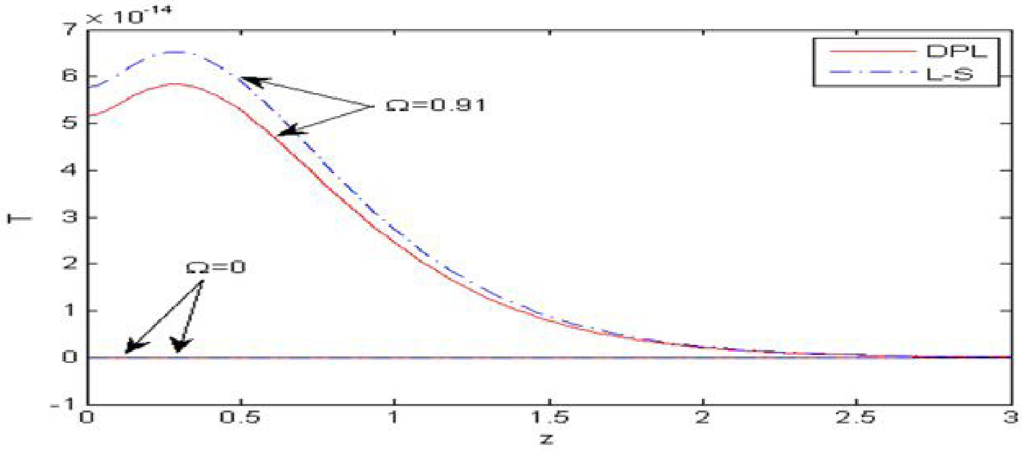


**Figure 4:** Variation of the temperature $T$ in the absence and presence of rotation

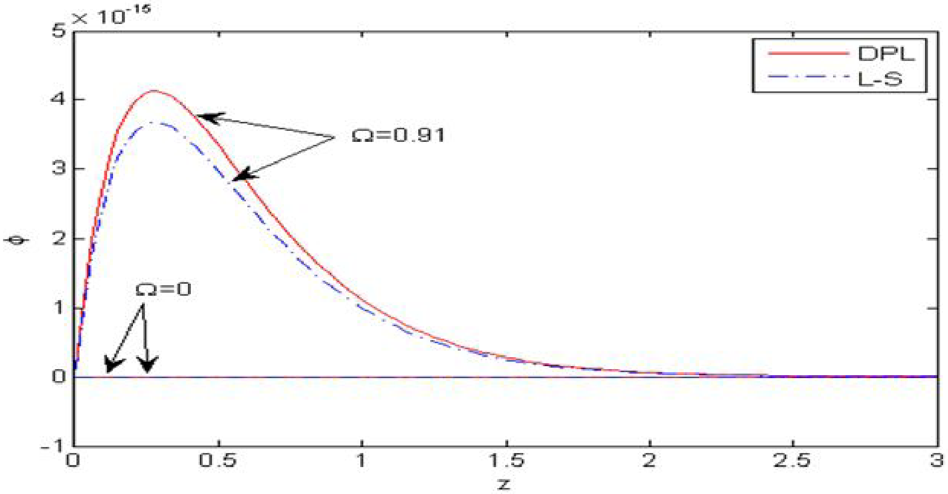


**Figure 5:** Variation of the micro-elongational scalar $\varphi$ in the absence and presence of rotation

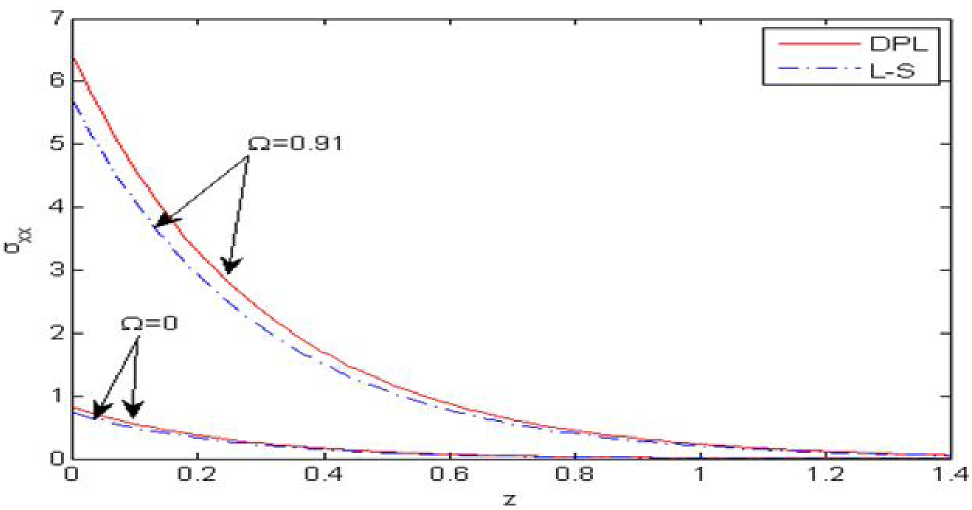


**Figure 6:** Variation of the force stress component $\sigma_{xx}$ in the absence and presence of rotation.

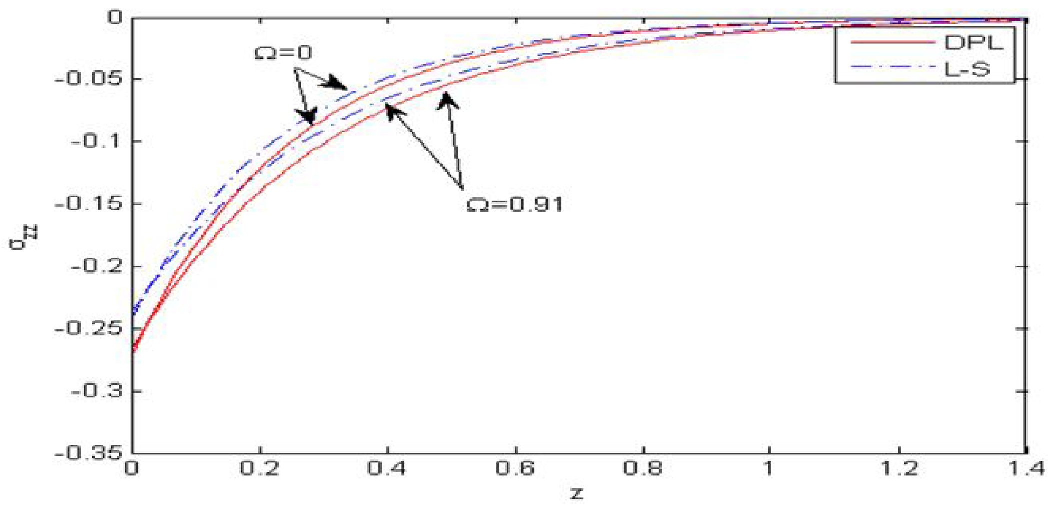


**Figure 7:** Variation of the force stress component $\sigma_{zz}$ in the absence and presence of rotation

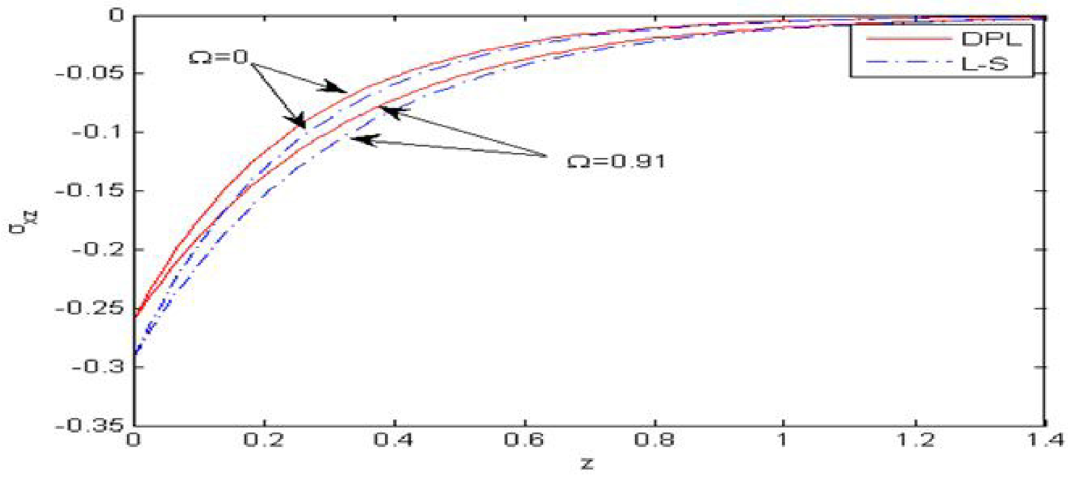


**Figure 8:** Variation of the force stress component $\sigma_{xz}$ in the absence and presence of rotation

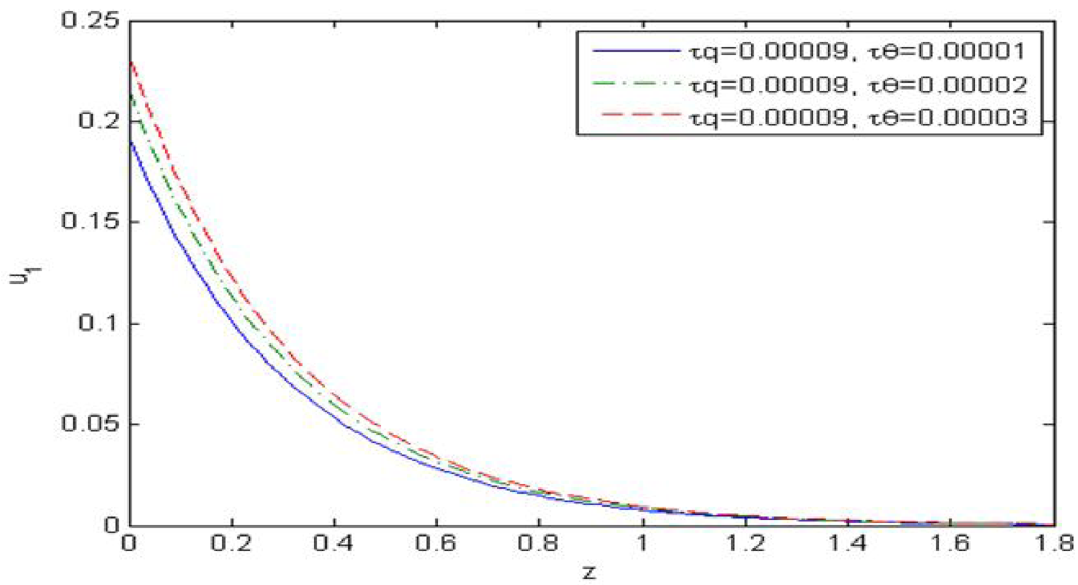


**Figure 9:** Variation of the horizontal displacement $u_1$ with distance $z$ in the presence of rotation.

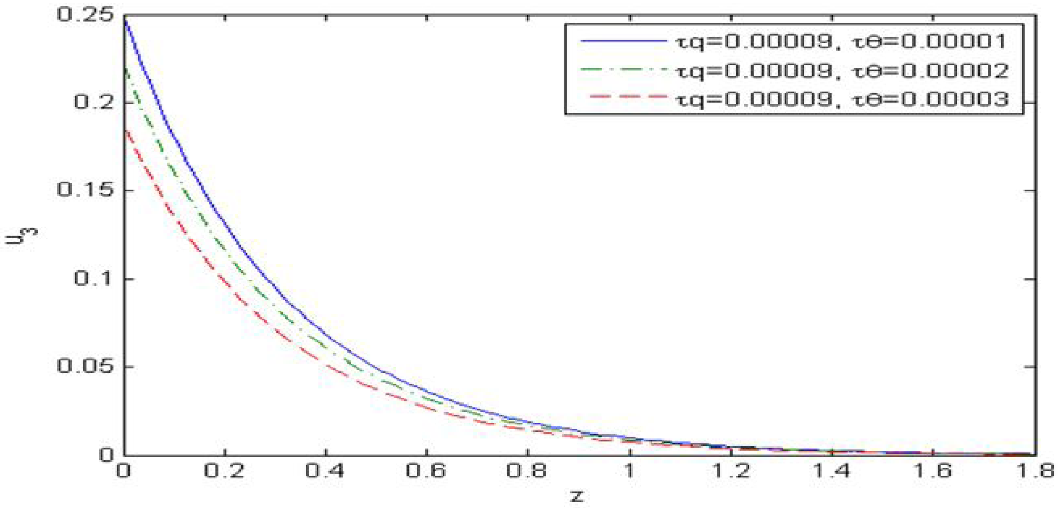


**Figure 10:** Variation of the vertical displacement $u_3$ with distance $z$ in the presence of rotation

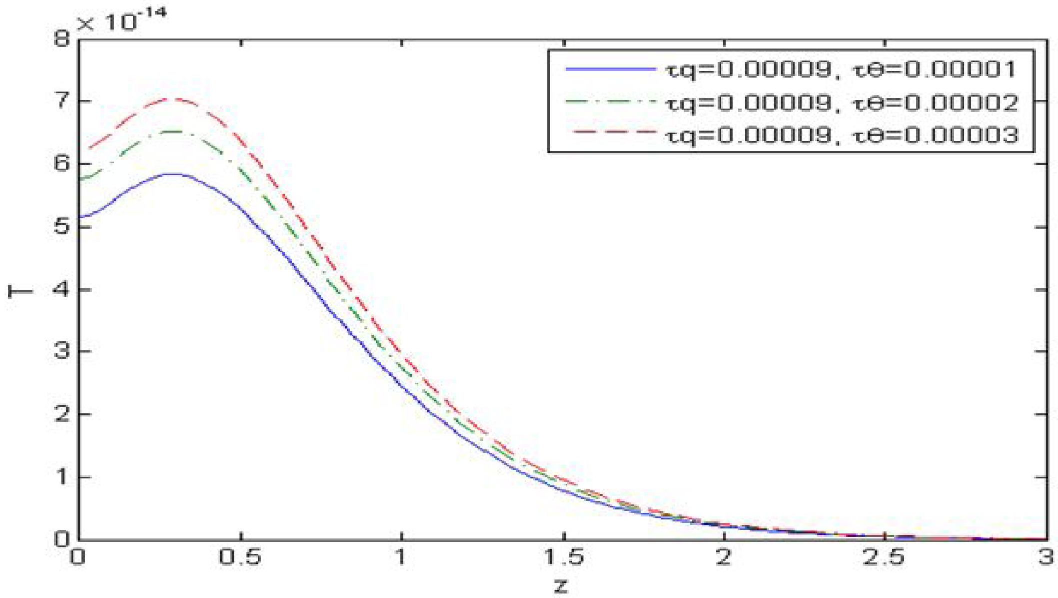


**Figure 11:** Variation of the temperature $T$ with distance $z$ in the presence of rotation.

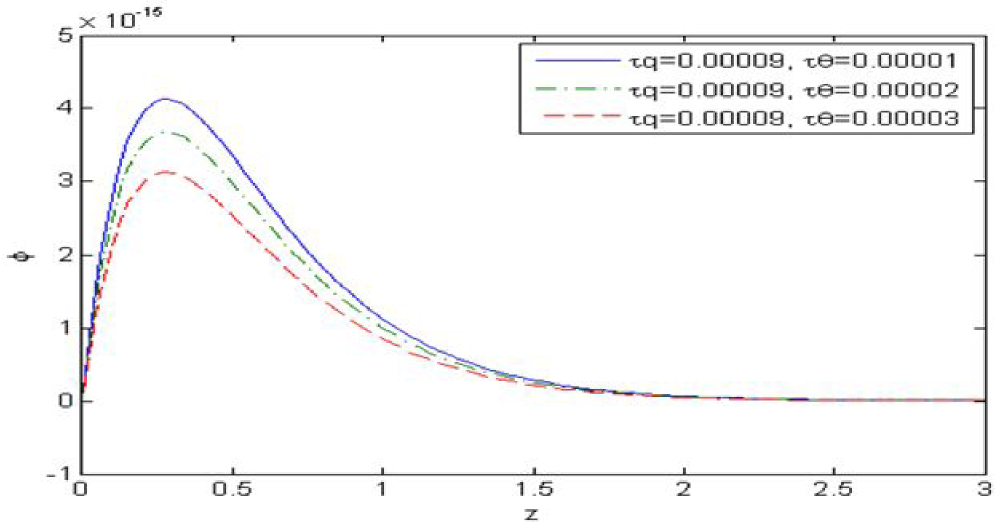


**Figure 12:** Variation of the micro-elongational scalar $\varphi$ with distance $z$ in the presence of rotation.

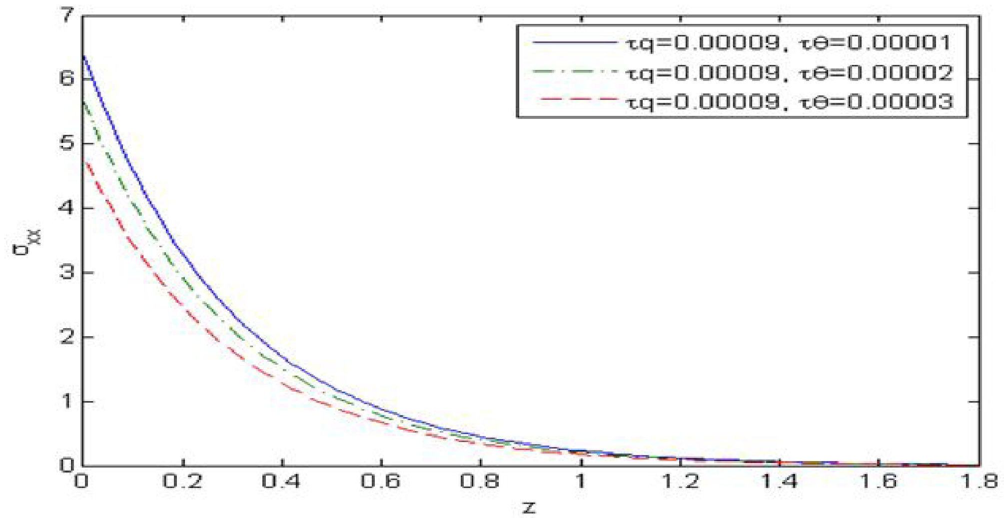


**Figure 13:** Variation of the force stress component $\sigma_{xx}$ with distance $z$ in the presence of rotation

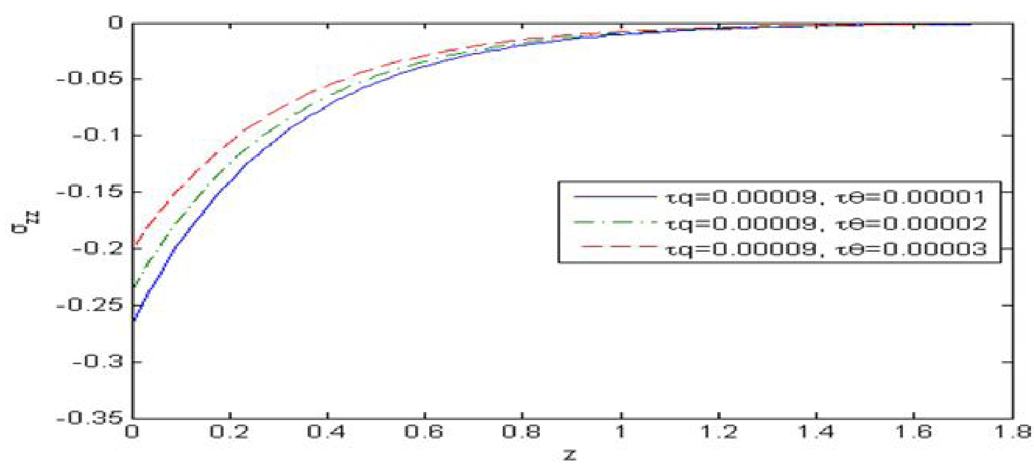


**Figure 14:** Variation of the force stress component $\sigma_{zz}$ with distance $z$ in the presence of rotation

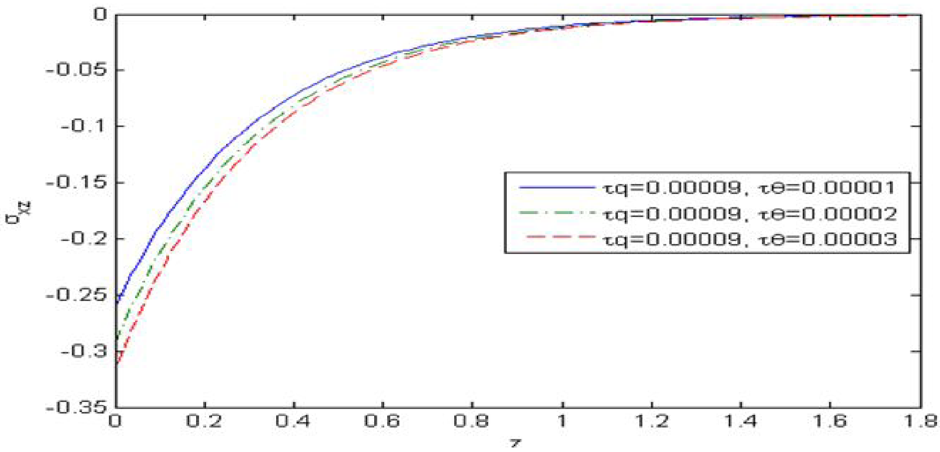


**Figure 15:** Variation of the force stress component $Z$ with distance $z$ in the presence of rotation.

## Conclusion

The method presented in this research applies to a wide range of thermodynamic problems. The current theoretical results may be of interest to experimental scientists' /researchers/ seismologists working in this subject. When the figures obtained under the two theories are compared, the following significant phenomena are observed:

1. The boundary conditions are satisfied by all physical quantities.
2. The physical quantities differ significantly between the DPL model and the L-S theory
3. The influence of rotation plays a big role in all physical quantities.
4. Recent interest in micro-elongated materials arises from their potential applications in smarter engineering structures.
5. Micro-elongated is presently experiencing a surge in basic research as well as technical applications.
6. The study of thermodynamic systems of bodies in equilibrium whose interactions with their surroundings are restricted to mechanical work, heat exchange, and external work is the focus of thermoelasticity.

## Rerefences

1. Othman MIA, Elmaklizi YD Ahmed EAA (2017) Effect of magnetic field on piezothermo-elastic medium with three theories Results Phys 7: 3361-3368.

2. Ashida F, Tauchert TR (1998) A finite difference scheme for inverse transient piezo-thermo-elasticity problems. J Therm Stress 21: 271-293.

3. Haussühl S, Bohatý L, Becker P (2006) Piezoelectric and elastic properties of the nonlinear optical material bismuth triborate, BiB3O6. Appl Phys A 82: 495-502.

4. Li D, He T (2018) Investigation of generalized piezoelectric-thermoelastic problem with non-local effect and temperature-dependent properties. Heliyon, 4: e00860.

5. Shaw S, Mukhopadhyay B (2012) Periodically varying heat source response in a functionally graded microelongated medium. Appl Math and Comput 128: 6304-6313.

6. Shaw S, Mukhopadhyay B (2013) Moving heat source response in a thermoelastic micro-elongated solid. J Eng Phys and Thermophys 86: 716–722.

7. Sachdeva SK, Ailawalia P (2015) Plane strain deformation in thermoelastic microelongated solid. Civil and Environm Resear 7: 92-98.

8. Ailawalia P, Sachdeva SK, Pathania DS (2015) Plane strain deformation in a thermoelastic microelongated solid with internal heat source. Int J Appl Mech and Eng 20: 717-731.

9. Ailawalia P, Sachdeva SK, Pathania, DS (2016) Internal heat source in thermoelastic micro-elongated solid under green lindsay theory. J Theor and Appl Mech 46: 65-82.

10. Ailawalia P, Sachdeva SK, Pathania DS (2019) A two-dimensional problem on laser pulse heating in thermoelastic microelongated solid. Arch of Thermody 40: 69-85.

11. Kumar R, Miglani A, Rani R (2019) Axisymmetric problem of a microelongated thermo-elastic medium due to thermomechanical sources. Int J Theor and Appl Mech 4: 52-61.

12. Ailawalia P, Singla A (2019) A thermoelastic microelongated layer immersed in an infinite fluid and subjected to laser pulse heating. Mech and Mech Eng 23: 233-240.

13. Ozisik MN, Tzou, DY (1994) On the wave theory of heat conduction. J Heat Transf (ASME) 116: 526-535.

14. Tzou DY (1995) Experimental support for the lagging behaviour in heat propagation. J.Thermophys Heat Transf 9: 686-693.

15. Tzou DY (1995) A unified field approach for heat conduction from macro- to micro-scales, J.Heat Transfer (ASME) 117: 8-16.

16. Othman MIA, Abd-Elaziz EM (2015) The effect of thermal loading due to laser pulse in generalized thermoelastic medium with voids in dual phase lag model. J Therm Stress 38: 1068-1082.

17. Abbas IA (2015) A dual phase lag model on thermoelastic interaction in an infinite fiber-reinforced anisotropic medium with a circular hole. Mech Based Design of Struct and Mach. 43: 501-513.

18. Abd-Alla AM, Othman MIA, Abo-Dahab SM (2016) Reflection of plane waves from electro-magneto-thermoelastic half-space with a dual-phase-lag model. Comput Mater Continua 51:63-79.

19. Othman MIA, Abd-Elaziz EM (2017) Effect of rotation on a micropolar magneto-thermo-elastic solid in dual-phase-lag model under the gravitational field. Microsy Tech 23: 4979-4987.

20. Othman MIA, Eraki EEM (2018) Effect of gravity on generalized thermoelastic diffusion due to laser pulse using dual-phase-lag model. Multi Model in Mater and Struct 14: 457-481.

21. Abdou MAA, Othman MIA, Tantawi RS, Mansour NT (2018) Effect of rotation and gravity on generalized thermoelastic medium with double porosity under L-S theory. J Mater Sci and Nanotech 6: 304-317.

22. Othman MIA (2004) Effect of rotation on plane waves in generalized thermoelasticity with two relaxation times. Int J Sol and Struct 41: 2939-2956.

23. Othman MIA (2005) Effect of rotation and relaxation time on a thermal shock problem for a half-space in generalized thermo-viscoelasticity. Acta Mech 174: 129-143.

24. Othman MIA, Singh B (2007) The effect of rotation on generalized micropolar thermo-elasticity for a half-space under five theories. Int J Sol and Struct 44: 2748-2762.

25. Othman MIA, Song Y (2008) Effect of rotation on plane waves of generalized electro- magneto-thermoviscoelasticity with two relaxation times. Appl Math Model 32: 811-825.

26. Li C, Yu Y, Tian X (2016) Effect of rotation on plane waves of generalized electro-magneto-thermoelastics with diffusion for a half-space. J Therm Stress 39: 27-43.

27. Othman MIA, Abbas IA (2021) 2-D Problem of micropolar thermoelastic rotating medium with eigenvalue approach under the three-phase-lag model. Waves in Random and Complex Media.

28. Kyame JJ (1949) Wave propagation in piezoelectric crystals. J of the Acoust Soci of Amer 21: 159-167.

29. Hutson AR, White DL (1962) Elastic wave propagation in piezoelectric semi-conductors. J Appl Phys 33: 40-47.

30. Sharma JN, Kumar M (2000) Plane harmonic waves in piezo-thermoelastic materials. Ind J Eng and Mater Sci 7: 434-442.

31. Othman MIA, Ahmed EAA (2015) The effect of rotation on piezo thermoelastic medium using different theories. Struct Eng and Mech 56: 649-665.

## Appendix 1

$$a_1=\frac{\mu}{\rho c_1^2},\ a_2=\frac{\lambda+\mu}{\rho c_1^2},\ a_3=\frac{\beta_1\lambda_0 c_1^2}{a_0\beta_0\omega^{*2}},\ a_4=\frac{\lambda_1 c_1^2}{a_0\omega^{*2}},\ a_5=\frac{\lambda_0^2}{a_0\rho\omega^{*2}},\ a_6=\frac{\rho j_0 c_1^2}{2a_0},\ a_7=\frac{\rho c_e c_1^2}{k\,\omega^*},\ a_8=\frac{\beta_0^2 T_0}{k\,\rho\omega^*},$$

$$a_9=\frac{\beta_1\beta_0 T_0 c_1^2}{k\,\lambda_0\omega^*},\ a_{10}=a_1+a_2,\ a_{11}=\Omega^2-\omega^2-a_{10}b^2,\ a_{12}=\Omega^2-\omega^2-a_1 b^2,\ a_{13}=a_5 b^2,\ a_{14}=b^2+a_4+a_6\omega^2,$$

$$a_{14}=b^2+a_4+a_6\omega^2,\ a_{15}=(1++\tau_q\omega),\ a_{16}=(1+\tau_\theta\omega),\ a_{17}=a_8a_{15}\omega,\qquad a_{18}=a_8a_{15}\omega b^2,\qquad a_{19}=a_{16}b^2+a_7a_{15}\omega,$$

$$a_{20}=\frac{\lambda+2\mu}{\rho c_1^2},\qquad a_{21}=\frac{\lambda}{\rho c_1^2},$$

$$A=\frac{1}{a_1a_{10}a_{16}}(a_1a_{17}-a_1a_5a_{16}-a_1a_{11}a_{16}+a_1a_{10}a_{19}-a_{10}a_{12}a_{16}+a_1a_{10}a_{14}a_{16}).$$

$$B=\frac{-1}{a_1a_{10}a_{16}}(-a_1a_{18}+a_{12}a_{17}-4a_{16}\omega^2\Omega^2+a_1a_{13}a_{17}+a_1a_5a_{19}+a_1a_{13}a_{16}+a_1a_{11}a_{19}-a_1a_{14}a_{17}-a_5a_{12}a_{16}-a_{11}a_{12}a_{16}+a_{10}a_{12}a_{19}$$
$$+a_1a_{11}a_{14}a_{16}-a_1a_{10}a_{14}a_{19}+a_{10}a_{12}a_{14}a_{16}+a_1a_5a_9\omega-a_1a_3a_9a_{10}\omega).$$

$$C=\frac{1}{a_1a_{10}a_{16}}(-a_{12}a_{18}+4a_{19}\omega^2\Omega^2-a_1a_3a_{18}+a_3a_{12}a_{17}-a_1a_{13}a_{19}+a_1a_{14}a_{18}+a_5a_{12}a_{19}+a_{12}a_{13}a_{16}+a_{11}a_{12}a_{19}-a_{12}a_{14}a_{17}$$

$$+4a_{14}a_{16}\omega^2\Omega^2-a_1a_{11}a_{14}a_{19}+a_{11}a_{12}a_{14}a_{16}-a_{10}a_{12}a_{14}a_{19}-a_1a_9a_{13}\omega+a_5a_9a_{12}\omega-a_1a_3a_9a_{11}\omega-a_3a_9a_{10}a_{12}\omega).$$

$$E=\frac{-1}{a_1a_{10}a_{16}}(a_{12}a_{14}a_{18}-a_{12}a_{13}a_{19}-a_3a_{12}a_{18}-4a_3a_9\Omega^2\omega^3-4a_{14}a_{19}\Omega^2\omega^2-a_{11}a_{12}a_{14}a_{19}-a_9a_{12}a_{13}\omega-a_3a_9a_{11}a_{12}\omega).$$

$$H_{2n}=\frac{-a_{17}k_n^4+(a_{18}+a_{14}a_{17}-a_5a_9\omega)k_n^2+(a_9a_{13}\omega-a_{14}a_{18})}{(a_{19}+a_{14}a_{16})k_n^2-a_{16}k_n^4-(a_{14}a_{19}+a_3a_9)},\ H_{3n}=\frac{a_5k_n^2-a_{13}-a_3H_{2n}}{(k_n^2-a_{14})},\ H_{1n}=\frac{2\Omega\omega}{a_1k_n^2+a_{12}}$$

$$H_{5n}=a_{20}k_n^2+iba_{20}k_nH_{1n}-b^2a_{21}-iba_{21}k_nH_{1n}-H_{2n}+H_{3n},$$

$$H_{6n}=-iba_1k_n+a_1k_n^2H_{1n}-iba_1k_n+a_1b^2H_{1n}$$

## Appendix 2

$$l_1=\frac{C_{44}}{C_{11}},\ l_2=\frac{C_{44}+C_{13}}{C_{11}},\ l_3=\frac{(e_{31}+e_{15})e_{33}}{\epsilon_{11}C_{11}},\ l_4=\frac{\rho^p c_0^2}{C_{11}},\ l_5=\frac{C_{33}}{C_{11}},\ l_6=\frac{e_{15}e_{33}}{\epsilon_{11}C_{11}},\ l_7=\frac{e_{33}^2}{\epsilon_{11}C_{11}}$$

$$G=\frac{1}{l_1l_7+l_1l_5l_{10}}(A_1l_7+A_2l_1l_{10}+A_1l_5l_{10}-b^2l_2l_3+b^2l_1l_6-b^2l_2^2l_{10}+b^2l_1l_5+b^2l_3l_5l_8+b^2l_1l_7l_9-b^2l_2l_7l_8)$$

$$N=\frac{1}{-l_1l_7-l_1l_5l_{10}}(-A_1b^2l_6-A_1A_2l_{10}+b^4l_2^2+b^4l_2l_3l_9-b^4l_1l_6l_9+b^4l_2l_6l_8-A_2b^2l_1-A_2b^2l_3l_8-A_1b^2l_5-A_1b^2l_7l_9)$$

$$F=\frac{1}{l_1l_7+l_1l_5l_{10}}(A_1A_2b^2+A_1b^4l_6l_9),\ L_{1m}=\frac{-l_1l_7r_m^4+l_1l_6b^2r_m^2+A_1l_7r_m^2-b^2l_2l_3r_m^2-A_1b^2l_6}{-ibl_2l_7r_m^3+ibl_3l_5r_m^3-ibl_3A_2r_m+ib^3l_2l_6r_m},$$

$$L_{1(m+3)}=\frac{-l_1l_7r_m^4+l_1l_6b^2r_m^2+A_1l_7r_m^2-b^2l_2l_3r_m^2-A_1b^2l_6}{ibl_2l_7r_m^3-ibl_3l_5r_m^3+ibl_3A_2r_m-ib^3l_2l_6r_m},\ L_{2m}=\frac{l_1r_m^2-A_1-ibl_2r_mL_{1m}}{ibl_3r_m},\ L_{2(m+3)}=\frac{l_1r_m^2-A_1+ibl_2r_mL_{1(m+3)}}{-ibl_3r_m}$$

$$L_{3m}=ib-l_{11}r_mL_{1m}-l_{12}r_mL_{2m},\ L_{3(m+3)}=ib+l_{11}r_nL_{1(m+3)}+l_{12}r_nL_{2(m+3)},\ L_{4m}=ibl_{11}-l_5r_mL_{1m}-l_7r_mL_{2m}$$

$$L_{4(m+3)}=ibl_{11}-l_5r_mL_{1(m+3)}-l_7r_mL_{2(m+3)},\ L_{5m}=-l_1r_m++ibl_1L_{1m}+ibl_6L_{2m},\ L_{5(m+3)}=l_1r_m++ibl_1L_{1(m+3)}+ibl_6L_{2(m+3)},$$

$$L_{6m}=-r_ml_9+ibl_9L_{1m}-ibL_{2m},\ L_{6(m+3)}=r_ml_9+ibl_9L_{1(m+3)}-ibL_{2(m+3)},\ L_{7m}=ibl_{13}-r_mL_{1m}+l_{10}r_mL_{2m},$$

$$L_{7(m+3)}=ibl_{13}+r_mL_{1(m+3)}-l_{10}r_mL_{2(m+3)}$$